NANO LETTERS

2001
Vol. 1, No. 11
595−600

Self-Assembled Honeycomb Networks of Gold Nanocrystals

Cynthia Stowell and Brian A. Korgel*

Department of Chemical Engineering, Texas Materials Institute and Center for Nano- and Molecular Science and Technology, The University of Texas, Austin, Texas 78712-1062

Received August 10, 2001

ABSTRACT

Size-monodisperse 35 Å diameter, sterically stabilized gold nanocrystals self-assemble into hexagonal networks, or two-dimensional honeycombs, during drop casting of a dispersion onto a substrate under the appropriate conditions. By changing the nanocrystal concentration prior to deposition, the microscopic morphology of self-assembled nanocrystal structures can be tuned from rings at high concentrations to honeycombs at low concentrations. The temperature dependence of the surface tension of the gold nanocrystal dispersions was measured using a ring tensiometer and found to depend on the particle concentration, particle size, and distribution. The morphological transition from rings to honeycombs appears to occur due to a transition from diffusive to convective fluid flow during solvent evaporation, which results directly from the surface tension and thermal conductivity differences between the dispersions.

In many instances, thermodynamics controls the structural organization of mesoscopic colloid-based materials. For example, size-monodisperse hard sphere colloids pack into face-centered cubic (fcc) superlattices;[1] charge-stabilized colloids and sterically stabilized nanocrystals can organize into fcc or bcc (body-centered cubic) lattices, depending on the range of repulsive interaction between particles;[2−5] and size-matched colloids with bimodal size distributions can form ordered phases, such as AB_{13} and AB_2 lattices.[6,7] The dynamics of the colloidal organization process, however, can also determine the structure of colloidal assemblies. Illustrative examples include the convective self-assembly of microscopically ordered colloidal arrays with macroscopic planar, spherical, ellipsoidal, and even doughnut shape.[8,9] Constraints imposed on the mobility of hard-sphere nanocrystals on a surface during monolayer deposition can frustrate equilibrium phase behavior. For example, disordered monolayers occur for zero surface diffusion (a process known as random sequential adsorption), a hexatic phase forms with limited surface diffusion, and the equilibrium phase (hexagonal array) forms when the surface mobility is high.[10] Ohara, Heath, and Gelbart have demonstrated the formation of organized rings of nanocrystals due to solvent dewetting effects during solvent evaporation.[11] More recently, Pileni and co-workers demonstrated the formation of a variety of microstructures, including polygonal networks of nanocrystals and rings, which were attributed to thermocapillary flow during evaporation.[12] In this letter, we describe our recent observation of self-assembled hexagonally organized networks of gold nanocrystals (see Figures 1d and 2a). The hexagonal networks consist of ribbons of nanocrystals approximately 15 nm thick and 500 nm wide; the honeycomb network has a lattice parameter L of $\sim$4.3 μm.

The microscopic morphology of the self-assembled structures depends on the starting nanocrystal concentration in the dispersion prior to deposition. Figure 1 shows the morphological progression that occurs with decreasing nanocrystal concentration prior to deposition, from rings to polygonal networks, to ordered hexagonal networks, and finally structures without microstructural order.

We ascribe the observed polymorphism to a transition from diffusive to convective fluid flow during evaporation. At high nanocrystal concentrations, thermocapillary flow does not occur and rings and polygonal networks form as a result of hole formation in the fluid upon evaporation and dewetting. Below a critical concentration, however, a Marangoni instability occurs giving rise to convective flow, which produces hexagonal networks under the appropriate conditions. The occurrence of the Marangoni instability depends on the temperature dependence of the surface tension, which was found to depend on the nanocrystal concentration and size.

Alkanethiol-stabilized gold nanocrystals were synthesized at room temperature using a modified version of the procedure developed by Brust et al.[13,14] Samples of relatively size-monodisperse 3.5 nm (Figure 2a) and 5 nm (Figure 2b) diameter nanocrystals and a polydisperse sample with sizes ranging from 3 to 12.5 nm diameters (Figure 2c) were studied.

* Corresponding author. Phone: (512) 471-5633. Fax: (512) 471-7060. E-mail: korgel@mail.che.utexas.edu.

10.1021/nl015601i CCC: $20.00
Published on Web 09/27/2001

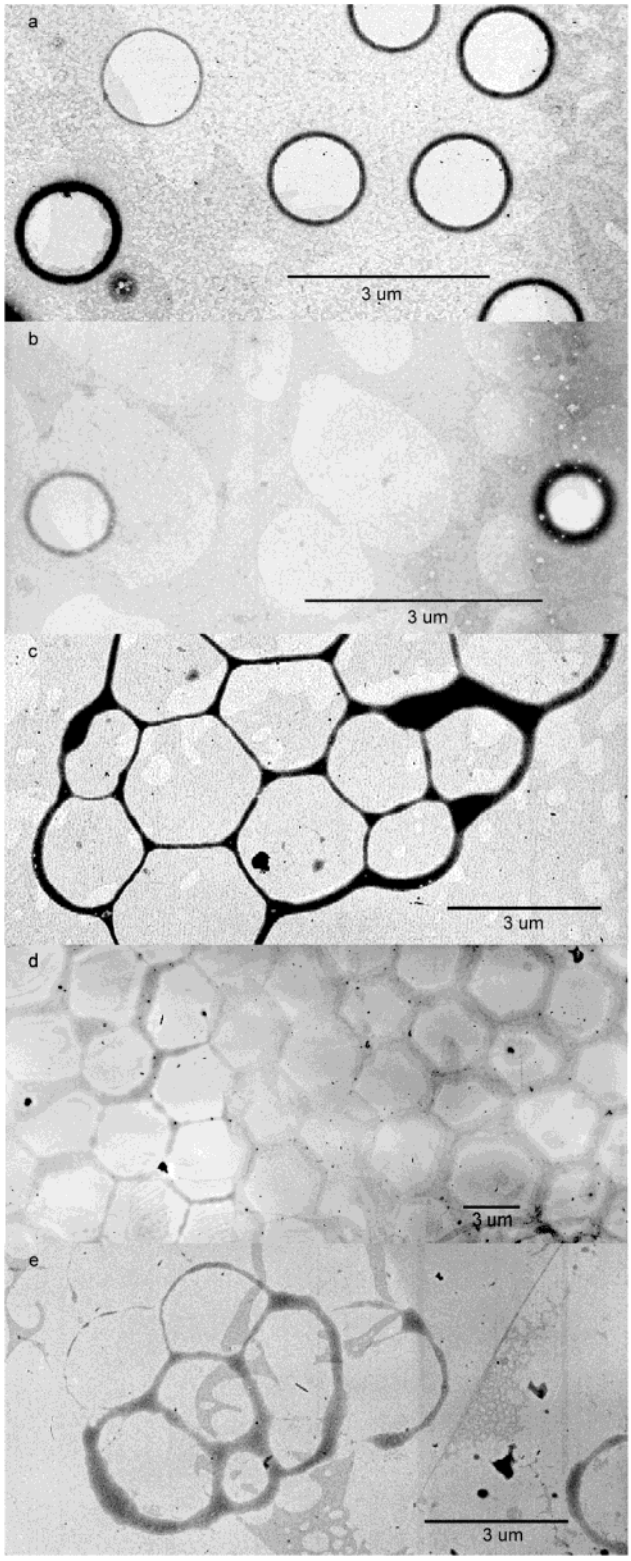

Figure 1. TEM images of microscopic structures formed by 35 Å diameter sterically stabilized Au nanocrystals drop-cast on a carbon substrate from a chloroform dispersion. (a) Au nanocrystals at 1.67 g/L deposit as rings. (b) At 0.277 g/L, the number of rings decreases. (c) At 9.26×10^{-2}, rings no longer form; instead, polygonal networks become the preferred morphology. (d) At 1.25×10^{-2} g/L, ordered repeating hexagonal networks resembling honeycombs dominate the structural morphology. (e) Further dilutions collapse the order.

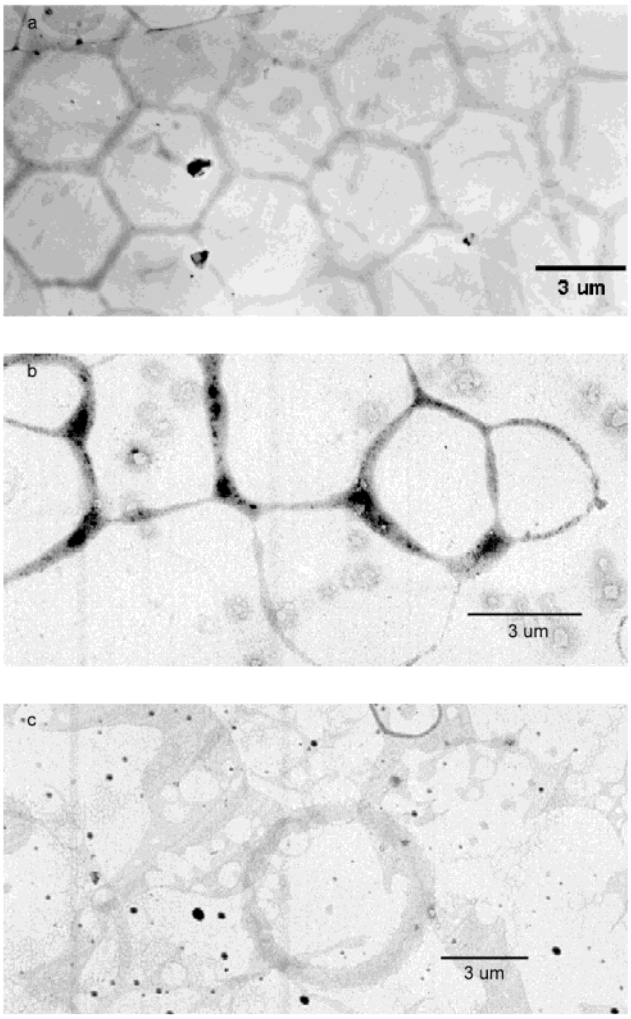

Figure 2. TEM images of (a) monodisperse 35 Å, (b) monodisperse 50 Å, and (c) polydisperse 30 to 125 Å Au nanocrystals deposited on a carbon substrate from chloroform at a concentration of 1.25×10^{-2} g/L.

Figure 3 shows a representative high-resolution transmission electron microscopy (TEM) image of the nanocrystals used. Note that the particles are separated on the substrate by ~15 Å, due to the stabilizing ligands that coat the nanocrystals and prevent uncontrolled aggregation in solution.

Dispersions were prepared with the following concentrations: 1.67 g of gold nanoparticles/L of chloroform, 2.8×10^{-1} g/L, 9.26×10^{-2} g/L, 1.25×10^{-2} g/L, and 1.25×10^{-3} g/L. Three μL of each nanocrystal dispersion was drop-cast on a carbon-coated 200 mesh copper TEM grid. The solvent was evaporated from the TEM grid while holding the substrate horizontal with anticapillary action tweezers at 20 °C in still air. The nanocrystal microstructures were imaged using a Phillips EM208 TEM operated at 120 kV acceleration voltage.

Figure 1 shows the progression of patterns formed with decreasing gold nanocrystal concentration for 3.5 nm diameter particles. At the highest concentration studied (1.67 g/L), the nanocrystals coalesce into ring structures with an average diameter of 1.7 μm. As the concentration is lowered

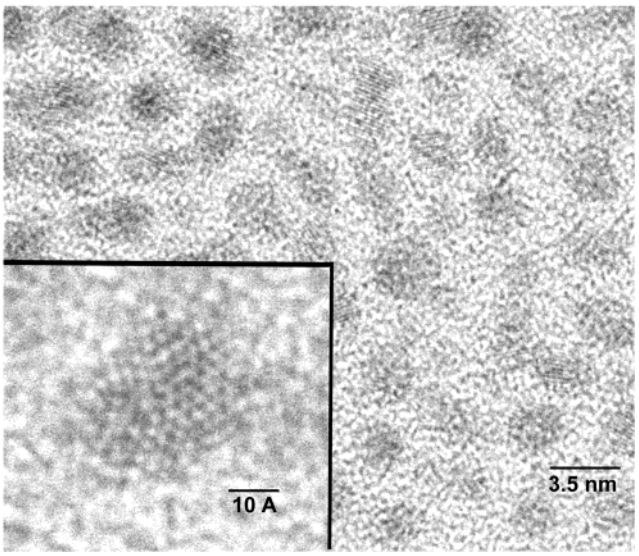

Figure 3. Representative high-resolution TEM image of Au nanocrystals used in the study.

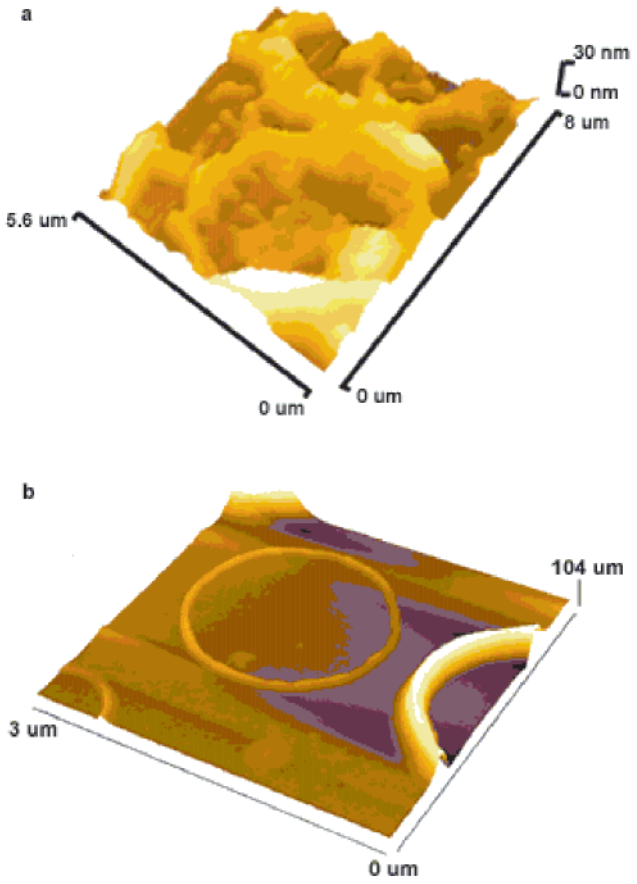

Figure 4. AFM images of (a) hexagonal networks and (b) dewetting rings of Au nanocrystals. The average height of the hexagonal borders are 15 nm, and the dewetting rings vary from 25 to 100 nm.

(9.26×10^{-2} g/L), the pattern transitions from isolated rings to polygon networks. As the nanocrystal concentration decreases further (1.25×10^{-2} g/L), the particles organize into networks of uniform hexagons as shown in Figure 1d, with a characteristic lattice parameter $L = 4.3$ μm. The characteristic size of the hexagonal networks formed using 35 Å diameter nanocrystals did not vary with nanocrystal preparation, the grid used, or the area on the grid examined. At concentrations below 1.25×10^{-2} g/L, the networks no longer appear, as in Figure 1e at a concentration of 1.25×10^{-3} g/L.

The nanocrystal size and size distribution affect the morphology of the self-assembled structures. Figure 2 shows representative TEM images of nanocrystal dispersions deposited from 1.25×10^{-2} g/L dispersions as a function of polydispersity and particle size. The larger 5 nm nanocrystals (Figure 2b) and the polydisperse nanocrystals (Figure 2c) with sizes ranging from 3 to 12.5 nm do not organize into hexagonal networks at this concentration, or at any of the other concentrations tested.

The thickness of the ring structures and the honeycomb networks was determined using atomic force microscopy (AFM; Thermomicroscopes Autoprobe CP Research). Figure 4 shows AFM images of the border of one of the hexagonal convection cells and nanocrystals that have formed a ring. The ring structures were significantly thicker than the honeycomb networks of particles, with heights of greater than 25 nm, compared to ~15 nm for the hexagonal borders.

Ohara, Heath, and Gelbart proposed that rings of nanocrystals form as a result of hole nucleation and growth in thin wetting solvents during evaporation.[11] In the absence of thermocapillary effects (i.e., convective motions in the fluid), the film thickness decreases homogeneously until reaching a critical thickness when the film becomes unstable and dewets the substrate through a hole nucleation mechanism. The critical thickness depends on the disjoining pressure of the solvent film on the substrate. The holes grow as solvent continues to evaporate. As a hole widens in the film, nanocrystals collect at the air-solvent interface until becoming "pinned" on the substrate. The solvent continues to evaporate, leaving the nanocrystals fixed on the substrate in the form of a ring. The separation between the hole nucleation event, which occurs at a critical fluid film height, and hole growth leads to relatively size-monodisperse ring diameters as shown in Figure 1a. Dewetting rings similar to these have also been observed for thin polymer films.[15] As the nanocrystal concentration decreases from 1.67 g/L, the evaporating hole spreads further before nanocrystal pinning occurs. At 9.26×10^{-2} g/L, the holes grow large enough to intersect. At the intersection of the rings, the nanocrystals restructure to minimize their interfacial free energy, resulting in the formation of polygonal networks. This dewetting mechanism has also been well documented for thin polymer films.[15]

Further decreases in the nanocrystal concentration (1.25×10^{-2} g/L) lead to the formation of organized hexagonal networks. It is highly unlikely that the hexagonal networks form as a result of intersecting dewetting holes. The thermodynamic packing constraints and force-field interactions between particles are not sufficiently complex or long-range to control microstructural organization into honeycomb networks. In essence, there is no driving force to spatially correlate neighboring dewetting holes into a hexagonal

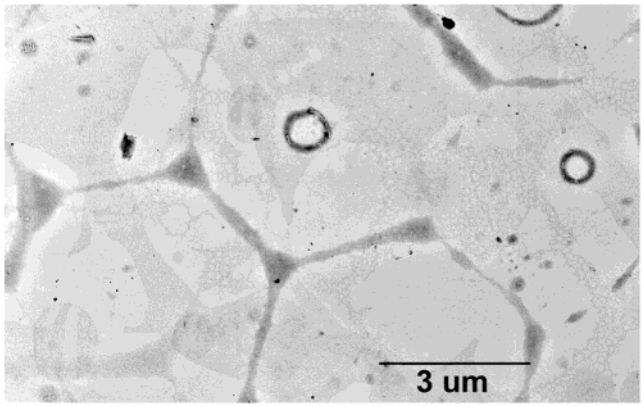

Figure 5. TEM image reveals dewetting rings within the honeycomb network.

lattice. In fact, organized hexagonal networks have not been observed in any dewetting thin polymer films—only disorganized polygonal networks have been formed.[15] Additionally, as seen in Figure 5, rings were observed within hexagonal cells, indicating that the rings and hexagons most likely do not both result from dewetting phenomena. The simultaneous occurrence of these patterns within the same cells indicates that they form at different stages of the evaporation process and that two different organizing mechanisms could be active under these deposition conditions.

Pileni and co-workers recently stated that Marangoni convection, or thermocapillary flow, can direct nanocrystal organization during the evaporation process.[12] In relatively thin fluid films, on the order of micrometers thick, solvent surface tension fluctuations at the air-solvent interface caused by a vertical temperature gradient across the film can give rise to two-dimensional hexagonally organized flow patterns.[16] As solvent evaporates from a drop-cast nanocrystal dispersion, a vertical temperature gradient results as evaporation cools the free surface relative to the isothermal substrate. Marangoni convection, originally observed by Bénard in 1900[17] and later explained by Pearson in 1958,[18] can give rise to hexagonal honeycomb networks of convective flow cells.[16] For a flat liquid film with negligible thickness compared to its length and fixed temperatures at the top and bottom surface, the Marangoni number *Ma*, is

$$Ma = \frac{\sigma_T \Delta T d}{\rho \nu \kappa} \qquad (1)$$

where, σ is the liquid surface tension, ΔT is the temperature differential across the fluid film of thickness d, $\sigma_T = |d\sigma/dT|$, ρ is density, ν is kinematic viscosity, and κ is the thermal diffusivity. The Marangoni number is a ratio of the force due to the surface tension gradient and the viscous forces. For a system characterized by *Ma* less than a critical Marangoni number $Ma_c \cong 80$, heat transfer from the underlying hot surface to the cool air—liquid interface occurs by diffusion. However, when $Ma > Ma_c = 80$, surface tension gradients become large relative to the viscous forces and convective motion sets in.[18,19] This instability in the fluid film can lead to a steady-state flow pattern of hexagonally

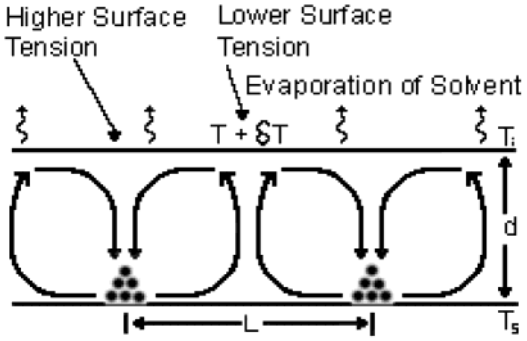

Figure 6. Illustration of surface tension driven convection. Solvent evaporation induces a vertical temperature gradient between the free gas—solvent interface and the relatively isothermal substrate. When $Ma > Ma_c$, the film becomes unstable to thermal fluctuations on the surface and convection occurs. The surface tension increases with decreasing temperature, causing the surface to spread at regions of higher temperature and contract at regions of lower temperature. The resulting surface flow forces warmer liquid near the substrate to rise and replace the spreading fluid, which leads to vertical convective flow. Flow is further enhanced because the rising fluid is warmer than the average gas—solvent interfacial temperature. Convection reaches steady state as viscous forces dissipate the surface tension induced energy gradient.

Table 1: Parameters Measured at 20 °C for 3.5 and 5 nm Gold Nanocrystals Dispersed in Chloroform: σ, σ_T, κ, *Ma*[a]

concentration (g/l)	diameter (nm)	σ (dynes/cm)	σ_T (dynes/cm·C)	κ (cm^2/s)	Ma
1.66	3.5	30.75	−0.5520	9.161×10^{-4}	63.6
2.77×10^{-1}	3.5	30.7	−0.5522	7.553×10^{-4}	77.1
9.26×10^{-2}	3.5	30.63	−0.5531	7.339×10^{-4}	79.5
1.25×10^{-2}	3.5	30.38	−0.5606	7.246×10^{-4}	81.6
1.25×10^{-3}	3.5	30.3	−0.6833	7.233×10^{-4}	99.7
1.66	5	29.94	−0.5421	9.161×10^{-4}	62.4
2.77×10^{-1}	5	29.85	−0.5447	7.553×10^{-4}	76.1
9.26×10^{-2}	5	29.8	−0.5496	7.339×10^{-4}	79
1.25×10^{-2}	5	29.77	−0.5520	7.246×10^{-4}	80.4
1.25×10^{-3}	5	29.67	−0.7392	7.233×10^{-4}	107.8

[a] For all solutions, $\rho = 1.471$ (g/mL), $\nu = 0.58$ cP, $\alpha = 1.24 \times 10^{-3}$ (1/K), $k = 2.46 \times 10^{-4}$ (cal/s·cm^2·(C/cm)), $k_g = 5.624 \times 10^{-5}$ (cal/s·cm^2·(C/cm)).

organized convective "cells," depicted in Figure 6. Steady-state flow occurs as the viscous forces dissipate the thermally derived surface tension energy gradients in the film. This behavior has been well studied in a variety of micrometer thick fluid films.[19] In these systems, the dimensionless wavenumber $a_c = 2\pi d/L$ is on the order of 2 and relates the characteristic lattice spacing of the hexagonal network L to the fluid film thickness d.

Few measurements of the surface tension, density, and viscosity of nanocrystal dispersions exist. Therefore, to calculate *Ma* for the dispersions, ρ, ν, and σ were measured as a function of nanocrystal concentration, size, and size distribution. Table 1 lists the parameters measured at 20 °C for 3.5 and 5 nm diameter gold dodecanethiol-capped nanocrystals at different concentrations in chloroform. There was no noticeable concentration dependence on ν.[20] The same was true for ρ—as expected for these dilute colloidal dispersions. However, σ (30.7 dyn/cm) for 1.66 g/L 3.5 nm and (29.94 dyn/cm) for 5 nm gold nanocrystals in chloroform at 20 °C exceeded the pure chloroform value of 27.4 dyn/

cm.[21] The surface tension increases with increasing particle concentration for both particle sizes. The increase in surface tension with increased concentration presumably results from the much lower volatility of the nanocrystals relative to the solvent. Values of σ_T also change significantly with particle concentration, with larger σ_T at lower concentrations. The increased solvent exposure at the air−liquid interface in more dilute nanocrystal dispersions leads to greater σ_T. The thermal conductivity also changes with nanocrystal concentration.[22] Changes in the thermal conductivity manifest themselves in *Ma* as variations in κ.

Ma was calculated using the measured parameters for each dispersion and estimating $\Delta T = 4.5$ °C and d=1.3 μm (Table 1).[23] In all of the 3.5 nm nanocrystal dispersions, *Ma* is close to 80, the critical Marangoni number required for convective flow, and increases with decreasing concentration. At 1.25 $\times$ 10^{-2} g/L, the concentration that produces hexagons, *Ma* > 80 and Marangoni convection is expected. At the onset of thermocapillary flow, the fluid sweeps the nanocrystals into the boundary regions between neighboring flow cells. The solvent velocity at the cell boundaries must reach a boundary condition of zero. Furthermore, the temperature of the solvent between cells is lowest, which gives the lowest nanocrystal solubility in the solvent film. With sufficient concentration and slow diffusion compared to the evaporation rate, the nanocrystals remain fixed between flow cells as the solvent evaporates below the film thickness required to host short wavelength instabilities.[24] The hexagonal networks form using a narrow range of nanocrystal concentrations because Marangoni convection becomes more favorable with decreasing concentration while simultaneously there must be enough particles to fill the gaps between convection cells.

Ordered honeycomb networks were not observed for polydisperse nanocrystals or larger 5 nm diameter nanocrystals. The 5 nm diameter nanocrystal solutions do not exhibit values of σ_T as high as the smaller particles, leading to slightly lower *Ma*. Nonetheless, *Ma* > 80 for the two most dilute solutions (the 1.25 $\times$ 10^{-2} g/L sample is shown in Figure 2b), yet hexagons were not observed for either case. In the most dilute solution there are certainly not enough particles to leave a residue of the hexagons on the grid. Since the Marangoni number is barely above 80 for the 1.25 $\times$ 10^{-2} g/L solution (assuming $d = 1.3$ μm), the drive toward convective behavior is not as strong as the 3.5 nm nanocrystal case, requiring a larger d for Marangoni convection to occur; thus, the nanocrystals have more time to diffuse away from the interface as the solvent evaporates completely. Indeed, the deposited nanocrystal patterns for the 5 nm particles appear as though they are approaching the polygonal networks that exist for the smaller nanocrystal samples.

The polydisperse sample, as shown in Figure 2c, did not exhibit order at any of the concentrations tested. It is possible that these samples could not achieve organized convective flow patterns due to the presence of renegade larger particles that disturbed the surface tension "field" within their vicinity at the interface, thus preventing spatially correlated flow patterns to develop. In this respect, it appears that in addition to the value of *Ma*, the local uniformity in particles size and interaction on the grid are also important.

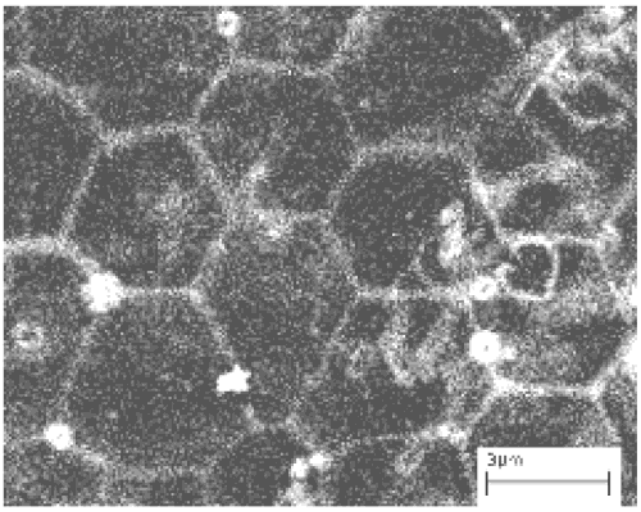

Figure 7. SEM image of a hexagonal network of 40 Å sterically stabilized nickel nanocrystals.

Other nanocrystals, in addition to gold, were also observed to form hexagonal networks, which confirms that this phenomenon is not just restricted to gold. For example, nickel particles with an average diameter of 4 nm produced honeycomb networks, as shown in the high-resolution SEM image of Figure 7.[25] In the sample, particle sizes ranged between 3 and 7 nm, yet networked hexagons formed. However, the ordering of this sample is less extensive than the gold nanoparticles, which can perhaps be attributed to the polydispersity of the nickel nanocrystals.

In conclusion, the experimental observations presented here demonstrate that, within a narrow concentration range, short wavelength Marangoni instability can occur during solvent evaporation to produce honeycomb networks of monodisperse sterically stabilized 3.5 nm diameter nanocrystals with a lattice parameter of 4.3 μm. Organized networks were not observed at higher nanocrystal concentrations, giving rise instead to 1.7 μm diameter rings as a result of the dewetting characteristics of the solvent. Rings have been observed to occur within the hexagonal networks, indicating that ring and hexagonal network formation occur at two different stages in the evaporation process.

A necessary but not sufficient condition for honeycomb network formation is that *Ma* > 80, which depends on the values of several parameters of the nanocrystal solution. The value of σ_T changes significantly as a function of particle concentration, with the most dilute solutions giving the largest changes. The combined changes in thermal conductivity and σ_T make the most dilute solutions more prone to Marangoni convection. However, the most dilute solutions do not form hexagonal networks because the particle concentrations are too low to leave significant deposits on the TEM grid. The particle size also affects σ_T, and 5 nm nanocrystals did not form hexagonal networks at concentrations identical to that of the 3.5 nm particles. Furthermore, nanocrystal polydispersity frustrates hexagonal network formation.

Acknowledgment. We thank J. Mendenhall and Glen Baum for assistance with TEM and surface tension measurements, respectively. We thank NSF, the Welch Foundation, and the ACS Petroleum Research Fund for supporting this work.

References

(1) Sanders, J. V. *Philos. Mag. A* **1980**, *42*, 705. (b) Alder, B. J.; Wainwright, T. E. *Phys. Rev.* **1962**, *127*, 359−361. (c) Pusey, P. N.; VanMegen, W. *Nature* **1986**, *320*, 340−342.

(2) (a) Luck, V. W.; Kleir, M.; Wesslau, H. *Ber. Bunsen-Ges. Phys. Chem.* **1963**, *67*, 75.

(3) McConnell, G. A.; Gast, A. P.; Huang, J. S.; Smith, S. D. *Phys. Rev. Lett.* **1993**, *71*, 2102−2105.

(4) Murray, C. B.; Kagan, C. R.; Bawendi, M. G. *Science* **1995**, *270*, 1335−1338.

(5) (a) Whetten, R. L.; Shafigullin, M. N.; Khoury, J. T.; Schaaff, T. G.; Vezmar, I.; Alvarez, M. M.; Wilkinson, A. *Acc. Chem. Res.* **1999**, *32*, 397−406. (b) Korgel, B. A.; Fitzmaurice, D. *Phys. Rev. B* **1999**, *59*, 14191−14201.

(6) (a) Sanders, J. V.; Murray, M. J. *Nature* **1978**, *275*, 201−203. (b) Bartlett, P.; Ottweill, R. H.; Pusey, P. N. *Phys. Rev. Lett.* **1992**, *68*, 3801−3804.

(7) (a) Kiely, C. J.; Fink, J.; Brust, M.; Bethell, D.; Schiffrin, D. J. *Nature* **1998**, *396*, 444−446. (b) Kiely, C. J.; Fink, J.; Zheng, J. G.; Brust, M.; Bethell, D.; Schiffrin, D. J. *Adv. Mater.* **2000**, *12*, 640.

(8) Denkov, N. D.; Velev, O. D.; Kralchevsky, P. A.; Ivanov, I. B.; Yoshimura, H.; Nagayama, K. *Langmuir* **1992**, *8*, 3183−3190.

(9) Velev, O. D.; Lenhoff, A. M.; Kaler, E. W. *Science* **2000**, *287*, 2240−2243.

(10) (a) Gray, J. J.; Klein, D. H.; Bonnecaze, R. T.; Korgel, B. A. *Phys. Rev. Lett.* **2000**, *85*, 4430−4433. (b) Gray, J. J.; Klein, D. H.; Korgel, B. A.; Bonnecaze, R. T. *Langmuir* **2001**, *17*, 2317−2328.

(11) (a) Ohara, P. C.; Heath, J. R.; Gelbart, W. M. *Angew. Chem., Int. Ed. Engl.* **1997**, *36*, 1077. (b) Ohara, P. C.; Gelbart, W. M. *Langmuir* **1998**, *14*, 3418−3424.

(12) (a) Maillard, M.; Motte, L.; Ngo, A. T.; Pileni, M. P. *J. Phys. Chem. B* **2000**, *104*, 11871−11877. (b) Maillard, M.; Motte, L.; Pileni, M. *Adv. Mater.* **2001**, *13*, 200−204.

(13) Brust, M.; Walker, M.; Bethell, D.; Schiffrin, D. J.; Whyman, R. *J. Chem. Soc. Chem. Commun.* **1994**, 801−802.

(14) All chemicals were used as supplied by the Aldrich Chemical Co. and all water was doubly distilled and deionized. 18 mL of a 30 mM aqueous solution of hydrogen tetrachloroaurate(III) hydrate ($HAuCl_4\,xH_2O$) was added to 12.5 mL of 0.2 M tetraoctylammonium bromide ($[CH_3(CH_2)_7]_4NBr$) in chloroform and stirred for 1 h. The organic phase was separated, and 120 μL of dodecanethiol was added. After stirring for 5 min, 15 mL of a 0.44 M aqueous solution of sodium borohydride ($NaBH_4$) was added. This solution was stirred for 12 h, and the organic phase again was collected. The resulting solution was alternately centrifuged in chloroform and ethanol three times to remove excess thiol, uncapped particles, and unused reactants. The 5 nm diameter nanocrystals (Figure 2b) were prepared in exactly the same manner as the 3.5 nm particles, except that the sodium borohydride solution was added approximately 5 s before the dodecanethiol. Polydisperse samples of gold nanocrystals with sizes ranging from 3 to 12.5 nm diameters (Figure 2c) were created by refluxing 3.5 nm diameter nanocrystals in toluene (1.5×10^{-5} g/μL) at 60 °C for 4 h.

(15) (a) Reiter, G. *Phys. Rev. Lett.* **1991**, *68*, 75−78. (b) Sharma, A.; Reiter, G. *J. Colloid Interface Sci.* **1996**, *178*, 383−399. (c) Thiele, U.; Mertig, M.; Pompe, W. *Phys. Rev. Lett.* **1998**, *80*, 2869−2872.

(16) Probstein, R. F. *Physiochemical Hydrodynamics: an Introduction*; Butterworths: Boston, 1989; pp 352−257.

(17) Bénard, H. *Rev. Gen. Sci. Pures Appl. Bull.* **1900**, *11*, 1261−1271.

(18) Pearson, J. R. A. *J. Fluid Mech.* **1958**, *4*, 489−500.

(19) Schatz, M. F.; VanHook, S. J.; McCormick, W. D.; Swift, J. B.; Swinney, H. L. *Phys. Rev. Lett.* **1995**, *75*, 1938−1941.

(20) A Cannon-Fenske viscometer was used to measure v.

(21) σ was measured using a ring tensiometer (Central Sceintific Co., Inc.) at 15.5 °C and 20 °C.

(22) To calculate the thermal diffusivity of each concentration, the mass fraction of gold relative to capping ligand was determined. The volume of gold was determined using the density of gold, and the volume contribution of the capping ligand was ignored. A volumetric average thermal diffusivity was calculated using the values for pure gold and pure chloroform.

(23) d was calculated using the relation $a_c = 2\pi d/L$, where dimensionless $a_c = 2$ at the onset of Marangoni convection. L was measured to be 4.3 μm. ΔT was measured experimentally by evaporating 3 μL of nanocrystal solution initially at 20 °C off of an Omega thermocouple.

(24) The diffusion coefficient of 3.5 nm nanocrystals was estimated using the Stokes−Einstein equation, $D_{AB} = kT/\mu_B 6\pi R_A$, where k is Boltzmann's constant, μ_B is the solvent viscosity, R_A is the nanocrystal radius, and T is the solvent temperature. Plugging in the appropriate parameters for these nanocrystals, $D_{AB} = 1.85 \times 10^{-10}$ m^2/s. A lower limit characteristic time for a 1.3 μm film to evaporate can be estimated by assuming no convection occurs in the gas phase: $\tau = \rho l \Delta x / D_{AB} \Delta c$; ρ is the density of chloroform, l is the stagnant diffusion film thickness (~0.2 μm), and Δc is the concentration gradient in the gas phase (9.4×10^{-4} g/cm^3). Considering a fluid film thickness $\Delta x = 1.3$ μm, $\tau = 2.05 \times 10^{-5}$ sec. Using this value of τ, the mean square displacement traveled by the nanocrystals during solvent evaporation can be estimated from $x = (4\pi D_{AB}\tau)^{1/2} = 0.22$ μm. Since $L = 4.3$ μm in the honeycomb arrays, the nanocrystals remain relatively localized during the final solvent evaporation.

(25) Nickel nanocrystals were synthesized in an argon environment by combining 0.211 g bis(cyclopentadienyl) nickel ($C_5H_6NiC_5H_6$), 480 μL of dodecanethiol, and 25 mL of toluene that was preheated to 75 °C. The solution was vigorously stirred at 75 °C for 2 h. The resulting solution was alternately centrifuged in chloroform and ethanol three times to remove excess thiol, uncapped particles, and reaction byproducts.

NL015601I